

[Click here to view linked References](#)

1 **Comparison of nickel adsorption on biochars produced from mixed**
2
3 **softwood and *miscanthus* straw**

4
5
6
7 Zhengtao Shen ^{a, b, 1, *}, Yunhui Zhang ^{a, 1}, Fei Jin ^c, Daniel S. Alessi ^b, Yiyun

8
9 Zhang ^a, Fei Wang ^{a, d, *}, Oliver McMillan ^a, Abir Al-Tabbaa ^a

10
11
12
13 ^a Geotechnical and Environmental Research Group, Department of
14 Engineering, University of Cambridge, Cambridge CB2 1PZ, United Kingdom

15
16
17
18 ^b Department of Earth and Atmospheric Sciences, University of Alberta,
19 Edmonton T6G 2E3, Canada

20
21
22 ^c School of Engineering, University of Glasgow, Glasgow G12 8QQ, UK

23
24
25
26 ^d Institute of Geotechnical Engineering, School of Transportation, Southeast
27 University, Nanjing 210096, China

28
29
30 * Corresponding author:

31
32 Zhengtao Shen, Email: ztshennju@gmail.com; zshen4@ualberta.ca

33
34 & Fei Wang, Email: 101012020@seu.edu.cn

35
36
37 ¹ These authors contributed equally to this work

1 Abstract: In order to understand the influence of feedstock type on biochar
2
3 adsorption of heavy metals, the adsorption characteristics of nickel (Ni^{2+}),
4
5 copper (Cu^{2+}) and lead (Pb^{2+}) onto biochars derived from mixed softwood and
6
7 *miscanthus* straw were compared. The biochars were produced from mixed
8
9 softwood pellets (SWP) and *miscanthus* straw pellets (MSP), at both 550 °C
10
11 and 700 °C for each material, using a standardised production procedure
12
13 recommended by the UK Biochar Research Centre. Kinetics analyses show
14
15 that the adsorption of Ni^{2+} to all four biochars reached equilibrium within 5
16
17 minutes. The degree of Ni^{2+} removal for all four biochars remained nearly
18
19 constant within initial pH values of 3-8, because the equilibrium pH values
20
21 within this range were similar due to the buffering effect of the biochars. A
22
23 sharp increase of Ni^{2+} removal percentage for all biochars at initial solution pH
24
25 8-10 was observed as the equilibrium pH also increased. MSP derived
26
27 biochars generally had higher maximum adsorption capacities (Q_{max}) for the
28
29 three tested metals as compared with those from SWP, which was likely due to
30
31 their higher degree of carbonisation during production. This study shows that
32
33 feedstock type is a primary factor affecting the adsorption capacities of the
34
35 tested biochars for heavy metals.
36
37
38
39
40
41
42
43
44
45
46
47
48
49
50

51
52
53 Keywords: biochar, remediation, adsorption, heavy metal, softwood,
54
55 *miscanthus* straw
56
57
58

1 Introduction

Environmental pollution in air, land, and water has been a huge challenge to the modern society (Hou and Li 2017; Qi et al. 2017; P. Zhang et al. 2017). The sustainable remediation of contaminated environmental media has drawn great attention during recent years (Hou and Al-Tabbaa 2014; Hou et al. 2017a; Hou et al. 2017b; Song et al. 2018). Biochar is regarded as an emerging and sustainable sorbent for heavy metal remediation of water and soil, due to its multiple additional environmental benefits including waste management, energy production, carbon storage and soil improvement (Ronsse et al. 2013; Lehmann 2007; Cao et al. 2011; Beesley et al. 2011; Shen et al. 2016; Shen et al. 2017a). Key to applying biochar for these purposes is an understanding of the adsorption characteristics of heavy metals, in order to aid in its practical application in water and soil remediation.

Biochar properties are highly dependent on the type of feedstock used (Zhang et al. 2017a). Plant, sewage sludge, manure and bones are raw materials often used for biochar production (Li et al. 2017), and plants obtained from agriculture wastes are among the most typical types of biomass used as biochar feedstock. Plants mainly consist of lignin, cellulose, hemicellulose and inorganic minerals, and the content of each component varies as a function of the plant type. Taking wood and wheat straw, two of the most frequently used

1 feedstocks for biochar, as examples, wood contains more lignin (25-30% for
2
3
4 wood versus 15-20% for wheat straw) and less inorganic minerals than does
5
6
7 straw (Jahirul et al. 2012). The differing thermal decomposition patterns of
8
9
10 each component during heating (Jahirul et al. 2012) results in biochars with
11
12 significantly different properties and consequently differing metal adsorption
13
14 behaviours. Heavy metal is an important class of environmental pollutants that
15
16
17 may originate from various anthropogenic sources and are widely distributed
18
19
20 (Hou et al. 2016, 2017c; Ma et al. 2015, 2014). A range of laboratory studies
21
22
23 have revealed the adsorption characteristics of heavy metals on biochars
24
25
26 produced from a particular plant biomass (e.g., Park et al. 2015; Shen et al.
27
28
29 2015; Chi et al. 2017). However, the biochar production parameters, including
30
31
32 highest heating temperature, heating rate, residence time, protection gas and
33
34
35 quality control, vary widely among these studies. It is therefore difficult to
36
37
38 isolate the influence of feedstock type on the adsorption of heavy metals by
39
40
41 biochar. Although comparison of the adsorption of heavy metals among
42
43
44 biochars, produced from different plant biomass under same conditions, has
45
46
47 been conducted in several previous studies (Wang et al. 2016; Mohan et al.
48
49
50 2007), it has not been extensively investigated, especially for biochars
51
52
53 produced under highly controlled pyrolysis conditions and having high
54
55
56 reproducibility.
57
58

1 In order to aid the selection of the most suitable biochars for treatment of
2
3 heavy metals in soil and water, it is critical to understand the influence of
4
5 feedstock type on biochar adsorption of heavy metals after eliminating other
6
7 influencing factors. To that end, in this study, mixed softwood and *miscanthus*
8
9 straw biochars were obtained from the UK Biochar Research Centre (UKBRC),
10
11 which aims to produce standardised biochars. A high degree of reproducibility
12
13 of these standard biochars can be achieved because the production process
14
15 and pyrolysis conditions are carefully monitored. This enables to isolate in the
16
17 current study the influence of feedstock type on biochar adsorption of three
18
19 tested metals: nickel (Ni^{2+}), copper (Cu^{2+}) and lead (Pb^{2+}), using laboratory
20
21 batch adsorption experiments.
22
23
24
25
26
27
28
29
30

31 32 33 2 Materials and methods 34 35

36 37 2.1 Biochar 38 39

40 Two types of feedstock biomass were used to produce the biochar used in this
41
42 study: (1) mixed softwood pellets (SWP) and, (2) *miscanthus* straw pellets
43
44 (MSP). Biochars were produced by the United Kingdom Biochar Research
45
46 Centre (UKBRC) from both SWP and MSP at both 550 °C and 700 °C,
47
48 resulting in four biochars hereafter referred to as SWP550, SWP700, MSP550
49
50 and MSP700. The standardised production procedure can be found on the
51
52 website of UKBRC (UKBRC 2016). Upon receipt, the biochars were dried in an
53
54
55
56
57
58
59

1 oven at 60 °C for 48 h and sieved to < 0.15 mm particle sizes before
2
3
4 experimentation. The cation exchange capacity (CEC) of each biochar was
5
6 tested using a compulsive exchange method based on Gillman and Sumpter
7
8 (1986). Other physicochemical properties were obtained from the UKBRC
9
10 (2016). The surface morphology of the biochar was examined by a scanning
11
12 electron microscopy (SEM) at 15 kV after coating the samples with gold. The
13
14 infrared spectrum of each biochar before and after Ni²⁺ adsorption was
15
16 obtained using a TENSOR II Fourier transform infrared spectroscopy (FT-IR)
17
18 spectrometer (Bruker), by taking 16 scans from 2000 to 700 cm⁻¹ with a
19
20 resolution of 1 cm⁻¹.
21
22
23
24
25
26
27
28

29
30 According to tests conducted by the UKBRC, the biochars predominantly
31
32 consist of carbon (75.41-90.21%) (Table 1). SWP derived biochars have
33
34 considerably lower pH than do those produced from MSP (7.91-8.44 versus
35
36 9.72-9.77). All four biochars are alkaline, with p_H_{pzc} (point of zero charge)
37
38 values between 7.8-7.9 (p_H_{pzc} values can be obtained from adsorption study
39
40 results of Mohan et al. (2014)). SWP derived biochars contain very low ash
41
42 content (1.25-1.89%), while the content in MSP biochars is much higher
43
44 (11.55-12.15%). Likewise, SWP derived biochars have lower P contents than
45
46 MSP (0.06-0.07% versus 0.19-0.76%). The CECs and surface areas of the
47
48 biochars are relatively low as compared with existing literature (Cui et al. 2015;
49
50
51
52
53
54
55
56
57
58
59
60
61
62
63
64
65

1 Chotpantararat et al. 2011), except for SWP700 which has a relatively high
 2
 3 surface area (162.30 m² g⁻¹) suggesting a porous structure.
 4
 5
 6

7 Table 1 Physicochemical properties of the biochars
 8
 9

	SWP550	SWP700	MSP550	MSP700
C (%)	85.52	90.21	75.41	79.18
H (%)	2.77	1.83	2.42	1.26
O (by difference) (%)	10.36	6.02	9.24	6.99
N (%)	<0.10	<0.10	0.78	1.03
P (%)	0.06	0.07	0.19	0.76
VM (%)	14.20	6.66	11.62	7.71
H:C	0.39	0.24	0.38	0.19
O:C	0.09	0.05	0.09	0.07
Total ash (%)	1.25	1.89	12.15	11.55
pH	7.91	8.44	9.77	9.72
pH _{pzc} *	7.8	7.9	7.8	7.8
BET surface area (m ² /g)	26.40	162.30	33.60	37.20
CEC (cmol/kg) *	2.53	2.56	5.95	10.80
Ni (mg/kg)	3.30	74.07	30.40	4.95
Cu (mg/kg)	19.41	9.66	26.64	5.88
Pb (mg/kg)	bdl	bdl	bdl	bdl

1 (VM = volatile matter, pH_{PZC} = point of zero charge, BET = Brunauer–Emmett–Teller, CEC
2
3
4 = cation exchange capacity, bdl = below detection limit, the standard deviations (SD) for
5
6 CEC were within 0.10-0.23, the SD for other properties can be found on UKBRC (2016),
7
8
9 note that all the values are obtained from the UKBRC datasheet, except for those denoted
10
11
12 with *)

15 2.2 Adsorption studies

16
17
18 Ni^{2+} , Cu^{2+} and Pb^{2+} were used as model divalent cations, to investigate the
19
20
21
22 sorption of heavy metals to these biochars. The kinetics and both the influence
23
24
25 of **adsorbent dosage** and solution pH on Ni^{2+} uptake from solution for all four
26
27
28 biochars were investigated. The equilibrium adsorption of Ni^{2+} , Cu^{2+} and Pb^{2+}
29
30
31 onto each of the biochars was also investigated.

32
33
34 Batch adsorption experiments were carried out in 50 mL polyethylene tubes in
35
36
37 a temperature-controlled laboratory (20 ± 1 °C). The detailed experimental
38
39
40 procedure of the adsorption studies can be found in Shen et al. (2017b). Briefly,
41
42
43 for kinetics studies, 0.1 g biochar was added to 20 mL solutions of 5 mM
44
45
46 $\text{Ni}(\text{NO}_3)_2$ (pH 5) (containing 0.01 M NaNO_3) and shaken at 200 rpm for 5 min,
47
48
49 10 min, 20 min, 30 min, 1 h, 2 h, 3 h, 6 h, 12 h or 24 h. The effect of **adsorbent**
50
51
52 **dosage** on the equilibrium adsorption of Ni^{2+} was investigated by adding a
53
54
55 measured amount of biochar (0.1, 0.2, 0.3, 0.4, 0.5, 0.6, 0.7, 0.8, 0.9 or 1 g) to
56
57
58 20 mL of 5 mM $\text{Ni}(\text{NO}_3)_2$ (containing 0.01 M NaNO_3) set to pH 5, and shaking

1 those mixtures at 200 rpm for 24 h. The effect of solution pH on Ni²⁺ adsorption
2
3 was investigated by adding 0.1 g of biochar to solutions containing 20 mL of 5
4
5 mM Ni(NO₃)₂ (containing 0.01 M NaNO₃), and subsequently shaking at 200
6
7 rpm for 24 h. The initial pH of each solution (before biochar addition) was
8
9 adjusted to 2, 3, 4, 5, 6, 7, 8, 9 or 10. Solutions of 0.01M, 0.1 M and 1 M HNO₃
10
11 and 0.01M, 0.1 M and 1M NaOH were used to adjust the initial pH of the
12
13 solutions where required. The equilibrium pH and the removal of Ni²⁺ were
14
15 recorded. In order to distinguish between precipitated Ni(OH)₂ and adsorbed
16
17 Ni²⁺ as a function of equilibrium pH, the fractions of Ni²⁺ removed via
18
19 precipitation were calculated using Visual MINTEQ 3.1.
20
21
22
23
24
25
26
27
28
29

30 In order to construct metal adsorption isotherms for each biochar, 0.1 g biochar
31
32 was added to 20 mL solutions (pH = 5) containing either Ni²⁺, Cu²⁺ or Pb²⁺, at
33
34 concentrations of 0.1, 0.2, 0.3, 0.5, 1, 2, 3 or 5 mM (containing 0.01 M NaNO₃).
35
36 The resulting mixtures were shaken at 200 rpm for 24 h to reach equilibrium.
37
38 The equilibrium data were fit using linearized Langmuir and Freundlich models
39
40 to reveal the maximum adsorption capacities and adsorption mechanisms of
41
42 the metals on the biochars, as suggested by (Foo and Hameed 2010). The
43
44 details of the models and calculations are given in Table S1.
45
46
47
48
49
50
51
52
53

54 2.3 Statistical analysis

55
56

57 All experiments were conducted in duplicates, and the means and standard
58
59

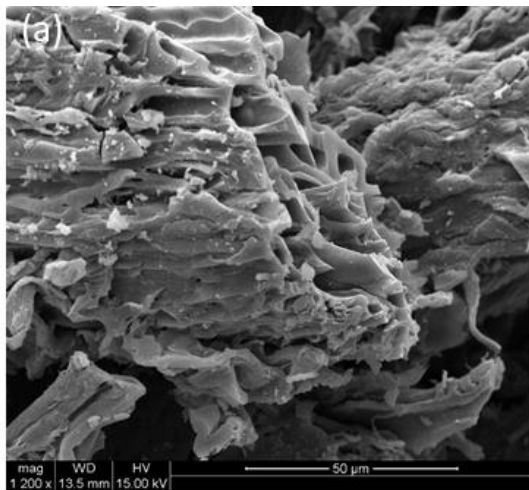
1 deviations were calculated from these data. Linear regression was used to
2
3 evaluate the fitness of the prediction models to the experimental data in this
4
5 study using Origin 8.5. The suitability of the model fitting was assessed using
6
7
8
9 R^2 values.
10

11 12 13 3 Results and discussion 14

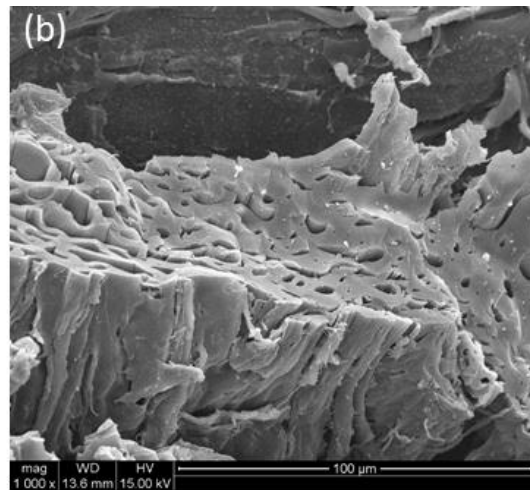
15 16 3.1 FT-IR spectra and SEM images of biochars 17

18
19 The FT-IR spectra of the biochars are shown in Fig. 5. The peaks at 1575 cm^{-1}
20
21 for SWP550 and MSP550 are attributed to aromatic C=C stretching (Keiluweit
22
23 et al. 2010), and the peaks at 875 , 800 and 750 cm^{-1} for SWP550 and MSP550
24
25 are attributed to aromatic C-H bending (Keiluweit et al. 2010), indicating an
26
27 aromatic structure of the two biochars. Less peaks associated with aromatic C
28
29 were observed on SWP700 and MSP700, suggesting that more condensed
30
31 aromatic structure with less functional groups was formed, as increased peak
32
33 temperature. The big peak between 1030 - 1080 cm^{-1} for MSP550 is attributed
34
35 to C-O-C stretching vibrations resulted from cellulose and hemicellulose
36
37 (Keiluweit et al. 2010). With increased peak temperature, cellulose and
38
39 hemicellulose in the *miscanthus* straw further decomposed, resulting in less
40
41 C-O-C groups. Therefore, this big peak diminished on FT-IR spectra of
42
43 MSP700. Wood typically contain less cellulose and hemicellulose and more
44
45 lignin than straw (Jahirul et al. 2012), therefore, the C-O-C peak was not
46
47
48
49
50
51
52
53
54
55
56
57
58
59
60
61
62
63
64
65

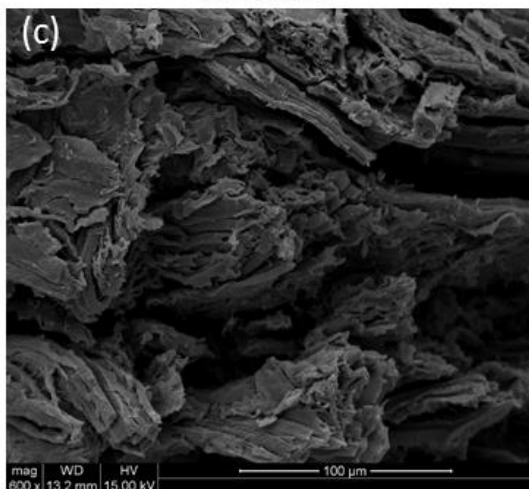
1 obvious for SWP derived biochars, or the cellulose and hemicellulose already
2
3 decomposed due to less amount. The SEM images (Fig. 1) show the porous
4
5 structures of the four biochars, which is typical for plant-derived biochars
6
7
8
9 (Usman et al. 2016). The pore diameters are generally less than 5 μm for all
10
11
12 biochars. MSP derived biochars generally reveal smaller pores than WSP. The
13
14 differences in the morphology due to production temperature were not
15
16
17
18 obvious.
19
20
21
22



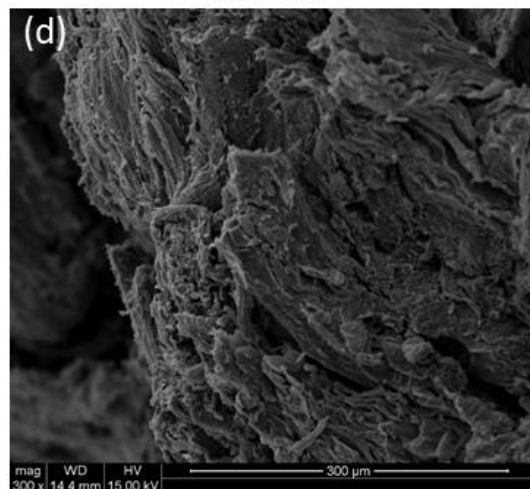
23
24
25
26
27
28
29
30
31
32
33
34
35
36
37
38
39
40 SWP550



41
42
43
44
45
46
47
48
49
50
51
52
53
54
55
56
57
58 SWP700



59
60
61
62
63
64
65 MSP550



11

1 Fig. 1. SEM images of the biochars, including: (a) SWP550, (b) SWP700, (c)
2
3 MSP550, and (d) MSP700.
4
5
6

7 3.2 Kinetics 8 9

10 The adsorption of Ni²⁺ to the four biochars reached equilibrium within 5
11 minutes (Fig. 2). Both the relatively high initial solution Ni²⁺ concentration (5
12 mM) and the fine biochar particle size (< 0.15 mm) likely contributed to this
13 rapid adsorption. Higher adsorbate concentration in solution results in a larger
14 chance for contact between the adsorbate and adsorbent surface, and
15 therefore accelerated movement of adsorbate across the external liquid film
16 boundary layer to external surface sites of the adsorbent (film diffusion) (Choy
17 et al. 2004). Smaller particles have larger **specific** surface area, which may
18 also aids the speed of film diffusion due to a larger solid – aqueous interface
19 (Choy et al. 2004). In addition, the mass transport of adsorbate inside the
20 adsorbent (intraparticle diffusion) becomes shorter as the radius of the
21 adsorbent particle decreases, which also makes the adsorption faster (Choy et
22 al. 2004; Rees et al. 2014). The rapid adsorption rate also suggests
23 chemisorption (e.g. surface precipitation) may be a predominant mechanism
24 for Ni²⁺ adsorption onto the four biochars, as chemisorption typically takes a
25 shorter time, often within minutes (Inyang et al. 2015; Saleh et al. 2016; Tran et
26 al. 2016).
27
28
29
30
31
32
33
34
35
36
37
38
39
40
41
42
43
44
45
46
47
48
49
50
51
52
53
54
55
56
57
58
59
60
61
62
63
64
65

1 The adsorption capacities (q_e) of Ni^{2+} on WSP550 and WSP700 were not
2 significantly different, with both values between 0.03 and 0.05 mmol/g. In
3
4
5
6
7
8
9
10
11
12
13
14
15
16
17
18
19
20
21
22
23
24
25
26
27
28
29
30
31
32
33
34
35
36
37
38
39
40
41
42
43
44
45
46
47
48
49
50
51
52
53
54
55
56
57
58
59
60
61
62
63
64
65

The adsorption capacities (q_e) of Ni^{2+} on WSP550 and WSP700 were not significantly different, with both values between 0.03 and 0.05 mmol/g. In contrast, the q_e values for MSP derived biochars were significantly higher. The q_e for MSP700, around 0.35 mmol/g, was nearly double that of MSP550, suggesting that a higher production temperature aids in the adsorption capacity of MSP derived biochars.

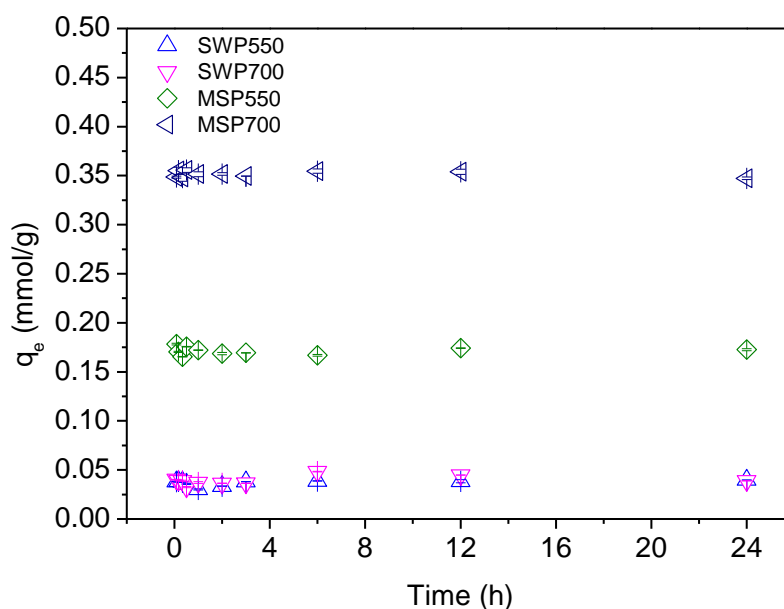


Fig. 2. Kinetics of Ni^{2+} adsorption on biochars (0.1 g biochar in 20 mL solution (0.01 M NaNO_3), initial Ni^{2+} concentration 5 mM; reaction temperature 20 °C; initial solution pH 5) (q_e - adsorption capacities).

3.3 Influence of adsorbent dosage

The influences of adsorbent dosage on Ni²⁺ removal and the adsorbed amount of Ni²⁺ per weight unit of biochar are shown in Fig. 3. The Ni²⁺ removal percentage for SWP550 increased from 3.97% to 16.63% across the adsorbent dosage range of 5-50 g/L. Likewise, the Ni²⁺ removal percentage for SWP700 increased from 3.89% to 20.54% at this range. Both biochars did not reach complete Ni²⁺ removal at the range of 5-50 g/L and exhibited low removal percentages compared with MSP derived biochars, suggesting a relatively low adsorption capacity of Ni²⁺ on SWP derived biochars. The adsorbed amount of Ni²⁺ per weight unit of biochar decreased in the range of 5-50 g/L for both of the SWP derived biochars.

In comparison to SWP derived biochars, the Ni²⁺ removal percentage for MSP550 increased from 17.28% to 98.03% as the adsorbent dosage increased from 5 to 40 g/L and remained at approximately 100% removal in the range of 40-50 g/L. The Ni²⁺ removal percentage for MSP700 increased from 18.29% to 99.67% at the adsorbent dosage range of 5-35 g/L and remained close to 100% removal up to 50 g/L. The adsorbed amount of Ni²⁺ per unit weight of biochar decreased as the adsorbent dosage increased from 5 to 50 g/L for both biochars. MSP-derived biochars generally show higher Ni²⁺ removal ability compared with SWP-derived biochars, which is in line with the

kinetics findings.

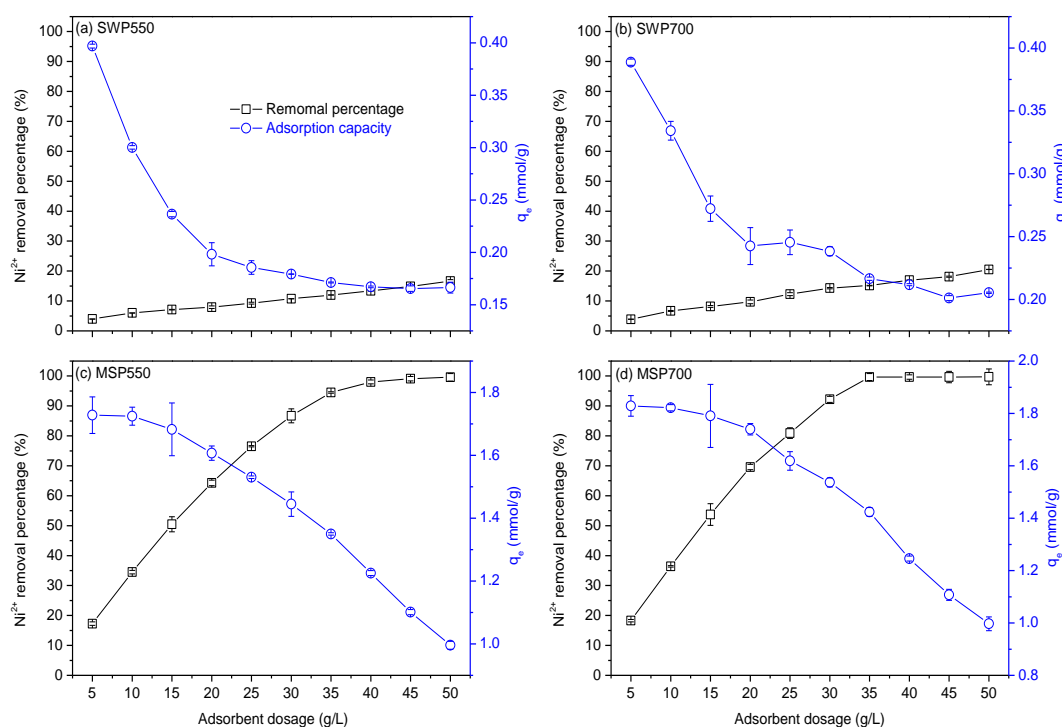


Fig. 3. The influence of adsorbent dosage on Ni²⁺ removal percentage and the adsorbed amount of Ni²⁺ per weight unit of biochar (mmol/g) (initial Ni²⁺ concentration 5mM in 20 mL solution (containing 0.01 M NaNO₃), reaction temperature 20 °C, initial solution pH 5, contact time 24 h).

3.4 Influence of solution pH

The influences of the initial solution pH on Ni²⁺ removal percentage and equilibrium solution pH values are shown in Fig. 4. The fraction of Ni²⁺ removed due to precipitation is also shown, which was calculated from the Ni(OH)₂ solubility data from the MINTEQ database. The high p_{H_{pzc}} (7.8-7.9)

1 suggests that the strong alkalinity of the biochars will aid in their adsorption for
2
3 heavy metals through surface precipitation. It is of note that the pH near the
4
5 biochar surface may be higher than the solution pH itself, and so even at lower
6
7 solution pH, surface precipitation of metals may already have occurred.
8
9 Therefore, there may be a discrepancy between the measured equilibrium
10
11 solution pH and the conditions of precipitation calculated using MINTEQ.
12
13
14
15
16

17
18 The Ni²⁺ removal percentage for SWP derived biochars was low (3-5%) in the
19
20 initial solution pH range of 2-7. It increased slightly to 9.82% at initial pH 8
21
22 before sharply increasing to 85.14% at initial pH 9 and subsequently increased
23
24 to 99.50% at initial solution pH 10 for SWP550. For SWP700, it stayed within
25
26 3-5% at pH 8 and sharply increased to 85.82% at pH 9. It further increased to
27
28 99.79% at initial pH 10. The Ni²⁺ removal percentage for MSP550 increased
29
30 from 3.41% to 15.44% as the initial solution pH increased from 2 to 4. It stayed
31
32 nearly constant at the initial pH range of 4-8 before significantly increasing to
33
34 98.45% at initial pH 9, and remained at nearly complete removal at initial pH
35
36 10. The Ni²⁺ removal percentage for MSP700 increased from 1.56% to 18.14%
37
38 with the increase of initial solution pH from 2 to 4. It was nearly constant within
39
40 the initial pH range of 4-7 and slightly increased to 33.33% at pH 8. A sharp
41
42 increase occurred between initial solution pH 8-9, nearing complete removal at
43
44 initial pH 9-10. The changes in the precipitation of Ni(OH)₂ did not have a
45
46
47
48
49
50
51
52
53
54
55
56
57
58
59
60
61
62
63
64
65

1 significant effect on Ni²⁺ removal between pH 2 and 9.
2
3

4 The Ni²⁺ removal percentages for SWP derived biochars were closely related
5
6
7 to the equilibrium solution pH values. The Ni²⁺ removal percentages remained
8
9
10 nearly constant within initial pH values of 3-8, because the equilibrium pH
11
12
13 values at this range were relatively stable resulting from the buffering effect of
14
15
16 the biochars. The insignificant increase of Ni²⁺ removal percentages at initial
17
18
19 pH 2-4 for SWP derived biochars was likely due to proton competition with Ni²⁺
20
21
22 for adsorption onto biochar surface functional groups (Uchimiya et al. 2012).
23

24 The sharp increase of Ni²⁺ removal percentage for all biochars at initial
25
26
27 solution pH 8-10 likely occurred because the p*H*_{pzc} values of the biochars were
28
29
30 exceeded. Under these conditions, the biochar surfaces became negatively
31
32
33 charged, which enhanced adsorption of Ni²⁺ through electrostatic interactions.
34

35
36 In addition, Ni(OH)₂ starts to precipitate on biochar surfaces at this range,
37
38
39 which likely also contributed to the sharp increase of Ni²⁺ removal from
40
41
42 solution.
43
44
45
46
47
48
49
50
51
52
53
54
55
56
57
58
59
60
61
62
63
64
65

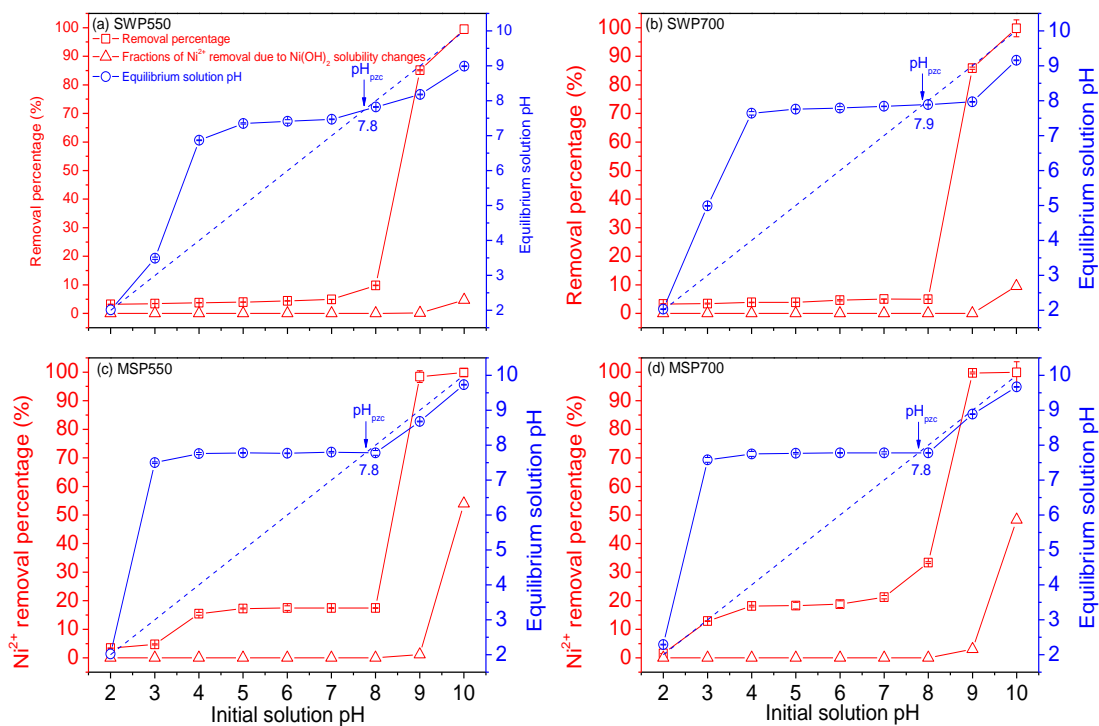


Fig. 4. The influence of initial solution pH on the Ni²⁺ removal percentage (red squares with solid lines), the equilibrium solution pH (blue circles with solid lines) and the fractions of Ni²⁺ removal due to the solubility change of Ni(OH)₂ (red triangles with solid lines); the dashed line is used to obtain the pH_{pzc} (initial Ni²⁺ concentration 5 mM, 0.1 g biochar in 20 mL solution (containing 0.01 M NaNO₃), reaction temperature 20 °C, contact time 24 h).

3.5 Adsorption equilibrium

Data from the equilibrium metal adsorption experiments conducted at room temperature for Ni²⁺ adsorption on biochars were modelled using isotherm approaches. Those for Cu²⁺ and Pb²⁺ were also obtained for comparison (Figs. S1, S2, S3 and Table 2). All isotherms are better fit by the Langmuir model

1 than by the Freundlich model, except for Ni²⁺ adsorption on MSP550 and
 2
 3 MSP700, indicating a monolayer adsorption of heavy metals on the biochars.
 4
 5 Ni²⁺ adsorption on MSP550 and MSP700 reveals slightly higher R² values for
 6
 7 the Freundlich model than for the Langmuir model, suggesting a certain degree
 8
 9 of heterogeneity of the adsorption sites on MSP550 and MSP700 surfaces.
 10
 11 The maximum adsorption capacity (Q_{max}) of heavy metals on biochars can be
 12
 13 calculated using the Langmuir model, and MSP derived biochars reveal
 14
 15 significantly higher Q_{max} values than do SWP for all three metals (Table 2).
 16
 17 Pb²⁺ generally has higher Q_{max} values than do Ni²⁺ and Cu²⁺ on the MSP
 18
 19 derived biochars, due to its lower hydration energy, which coincides with many
 20
 21 previous findings (Shen et al. 2015; Liu et al. 2013). For SWP derived biochars,
 22
 23 the Q_{max} values for the three metals vary considerably, and so there is not a
 24
 25 specific metal that has the highest Q_{max} values.
 26
 27
 28
 29
 30
 31
 32
 33
 34
 35
 36
 37
 38
 39
 40
 41
 42
 43
 44
 45
 46

39 Table 2 Parameters and regression coefficient of the equilibrium data for Ni²⁺,
 40
 41 Cu²⁺ and Pb²⁺ adsorption on the biochars fitted by the linear Langmuir and
 42
 43 Freundlich isotherm models.
 44
 45
 46

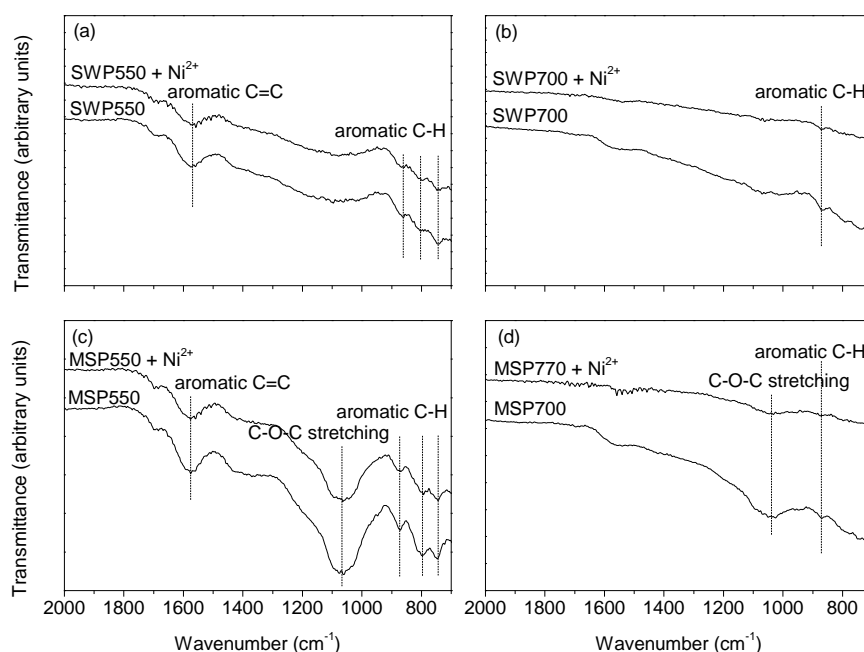
Metal	Biochar	Langmuir			Freundlich		
		Q _{max} (mmol/g)	b (L/mmol)	R ²	K _f	1/n	R ²
Ni ²⁺	SWP550	0.057	0.535	0.979	0.018	0.540	0.959

	SWP700	0.043	1.821	0.963	0.024	0.353	0.954
	MSP550	0.157	161.579	0.865	0.146	0.157	0.899
	MSP700	0.196	123.481	0.682	0.179	0.145	0.699
	SWP550	0.019	13.321	0.999	0.017	0.088	0.955
	SWP700	0.086	4.785	0.985	0.061	0.226	0.980
Cu ²⁺	MSP550	0.130	133.062	0.999	0.112	0.103	0.275
	MSP700	0.229	351.633	0.994	0.198	0.233	0.343
	SWP550	0.039	33.437	0.999	0.037	0.081	0.904
	SWP700	0.079	909.290	0.9999	0.074	0.079	0.375
Pb ²⁺	MSP550	0.183	-407.054	0.9998	0.164	0.151	0.467
	MSP700	0.357	23.907	0.998	0.318	0.315	0.451

3.6 Adsorption mechanisms and discussion

Biochar can adsorb heavy metals through a range of mechanisms including physical sorption, cation exchange, cation- π interaction, surface complexation and surface precipitation (Shen et al. 2017b). The FT-IR spectra (Fig. 5) generally show slight decrease of the peaks representing aromatic C=C and aromatic C-H of all four biochars after Ni²⁺ adsorption. This suggests that

1 cation- π interaction, which is closely related to aromatic C (Keiluweit and
2
3
4 Kleber 2009), may be a mechanism for Ni^{2+} adsorption on the four biochars.
5
6
7 The peaks representing C-O-C stretching also decreased after Ni^{2+} adsorption
8
9
10 for MSP derived biochars. This C-O-C belongs to acid derivatives (Keiluweit
11
12 2010), suggesting cation exchange or complexation, associated with acidic
13
14
15 groups, may also contribute to Ni^{2+} adsorption on MSP derived biochars.
16
17
18
19
20



21
22
23
24
25
26
27
28
29
30
31
32
33
34
35
36
37
38
39
40
41
42
43
44
45 Fig. 5. FT-IR spectra of biochars before and after Ni^{2+} adsorption (the post Ni^{2+}
46
47 adsorption sample was obtained from those for isotherm tests at 5 mM).
48
49
50

51
52 A previous study observed that surface precipitation and cation- π interaction
53
54 are the main mechanisms contributing to heavy metal adsorption for biochars
55
56 produced from other feedstocks (wheat straw and rice husk) but under the
57
58
59
60
61
62
63
64
65

1 same production processes as those used in the present study (Shen et al.
2
3 2017b). In the present study, the high solution-pH dependence of the
4
5 adsorption capacity of the four biochars for Ni²⁺ (Fig. 4) suggests that surface
6
7 precipitation or cation-π interaction are the primary adsorption mechanisms,
8
9 as they are both highly pH-dependent. As mentioned above, wood typically
10
11 has higher lignin content than does *miscanthus*, but lower inorganic minerals.
12
13 The incomplete carbonation of the feedstock during production of biochar, due
14
15 to more ligneous material which is more thermally resistant, can result SWP
16
17 derived biochars with less alkaline minerals (e.g., K₂O) (Dodson 2011), as is
18
19 indicated by lower pH (Table 1) as well as in lower contents of inorganic
20
21 compounds (e.g. CO₃²⁻ and PO₄³⁻) for metal precipitation.
22
23
24
25
26
27
28
29
30

31
32 Therefore, SWP derived biochars may have adsorbed Ni²⁺ through surface
33
34 precipitation and cation-π interaction. In comparison, MSP derived biochars
35
36 may have stronger ability to precipitate Ni²⁺ compared with SWP. MSP derived
37
38 biochars may also adsorb Ni²⁺ through cation exchange and surface
39
40 complexation, in addition to precipitation and cation-π interaction. Therefore,
41
42 SWP derived biochars have lower adsorption capacities for Ni²⁺ and other two
43
44 metals as compared with MSP. This indicates that feedstock type is an
45
46 important factor affecting the adsorption capacities of biochars for heavy
47
48 metals.
49
50
51
52
53
54
55
56
57
58

1 For the same feedstock, a higher production temperature generally results in a
2
3
4 higher adsorption capacity for the metals (Table 2). Higher production
5
6 temperature promotes the carbonisation process of the feedstock and
7
8 therefore aids the formation of more alkaline minerals, which will aid in the
9
10 precipitation of metals to biochar surfaces. Although the pH and ash content
11
12 were not significantly different between MSP550 and MSP700, the significantly
13
14 lower O/C and H/C values for MSP700 suggests a higher degree of
15
16 carbonisation and a higher aromaticity, which could provide MSP700 more
17
18 aromatic π electrons for cation- π interactions with the metals (Keiluweit and
19
20 Kleber 2009).
21
22
23
24
25
26
27
28

29
30 Apart from the adsorption capacity, the kinetics of metal uptake and the
31
32 influence of solution pH on the degree of metal adsorption are similar for SWP
33
34 and MSP derived biochars. Biochars produced from wheat straw and rice husk
35
36 under the same standardised production process in a previous study (Shen et
37
38 al. 2017c) also show similar trends in terms of kinetics and the influence of
39
40 solution pH to Ni^{2+} adsorption. The faster kinetics of removal may be due to the
41
42 small particle size of the biochars and the relatively high initial sorbate
43
44 concentrations in solutions in both of the two studies.
45
46
47
48
49
50
51

52 53 54 4 Conclusions 55 56

57 This study investigates the adsorption characteristics of Ni^{2+} , Cu^{2+} and Pb^{2+} on
58

1 SWP and MSP derived biochars. The kinetics study shows that the adsorption
2
3 of Ni²⁺ to all four biochars reached equilibrium rapidly (within 5 minutes),
4
5 regardless of feedstock type and production temperature, which may be due to
6
7 the small particle size of the biochars and relatively high initial sorbate
8
9 concentrations in solutions. Likewise, the solution-pH dependence of Ni²⁺
10
11 adsorption for the four biochars shows a similar trend. There was an initial
12
13 solution pH range of approximately 3-8, within which both the Ni²⁺ removal
14
15 percentage and equilibrium solution pH remained nearly constant. This was
16
17 due to a nearly constant equilibrium solution pH within the range, which
18
19 resulted from the buffering effect of the biochars. Between the initial solution pH
20
21 range of 8-10, the Ni²⁺ removal percentage dramatically increased to nearly
22
23 100%, corresponding to increased equilibrium solution pH. In general, the
24
25 adsorption of Ni²⁺ on the four biochars was highly dependent on equilibrium
26
27 solution pH. The biggest difference between the adsorption characteristics of
28
29 SWP and MSP derived biochars are their adsorption capacities for all three
30
31 metals. MSP derived biochars have significantly higher Q_{max} values than do
32
33 those produced from SWP. Lignin and inorganic mineral contents may be the
34
35 primary factors that cause the differences of adsorption capacity between
36
37 SWP and MSP derived biochars.
38
39
40
41
42
43
44
45
46
47
48
49
50
51
52
53

54 Our study indicates that feedstock type is a primary factor affecting the
55
56
57
58

1 adsorption capacities of biochar for heavy metals. As this study only includes
2
3 adsorption studies, the influence of feedstock type on the
4
5 desorption/reusability of the biochars are suggested for future work. More
6
7 testing methods (e.g., X-ray absorption and X-ray diffraction) and surface
8
9 complexation modelling may be used to aid in determining the mechanistic
10
11 driving forces impacting the adsorption capacities of biochar for heavy metals
12
13 in future studies.
14
15
16
17
18
19
20

21 Acknowledgements

22
23
24
25 The standard biochars were obtained from the UK Biochar Research Centre
26
27 (UKBRC) at the University of Edinburgh. The authors would like to thank Dr.
28
29 Ondrej Masek from the UKBRC for his kind help in preparing and delivering
30
31 the biochar samples. Special thanks also go to Dr. Zhen Li from the College of
32
33 Resources and Environmental Sciences, Nanjing Agricultural University, China,
34
35 who conducted the SEM imaging for the biochars used in this study. The
36
37 authors would also like to thank Tiesheng Wang and Rui Wu from the
38
39 Department of Materials Science and Metallurgy at the University of
40
41 Cambridge for conducting the FT-IR tests. The first author would like to thank
42
43 the Killam Trusts from Canada for kindly providing the Izaak Walton Killam
44
45 Memorial Postdoctoral Fellowship.
46
47
48
49
50
51
52
53
54
55
56
57
58
59
60
61
62
63
64
65

1 References
2
3

4 Beesley L, Moreno-Jiménez E, Gomez-Eyles JL, et al (2011) A review of
5
6 biochars' potential role in the remediation, revegetation and restoration of
7
8 contaminated soils. *Environ Pollut* 159:3269–82. doi:
9
10 10.1016/j.envpol.2011.07.023
11
12
13
14

15
16 Cao X, Ma L, Liang Y, et al (2011) Simultaneous immobilization of lead and
17
18 atrazine in contaminated soils using dairy-manure biochar. *Environ Sci*
19
20 Technol 45:4884–9. doi: 10.1021/es103752u
21
22
23
24

25
26 Chi T, Zuo J, Liu F (2017) Performance and mechanism for cadmium and lead
27
28 adsorption from water and soil by corn straw biochar. *Front Environ Sci*
29
30 Eng. doi: 10.1007/s11783-017-0921-y
31
32
33
34

35 Chotpantarat S, Ong SK, Sutthirat C, Osathaphan K (2011) Competitive
36
37 sorption and transport of Pb²⁺, Ni²⁺, Mn²⁺, and Zn²⁺ in lateritic soil
38
39 columns. *J Hazard Mater* 190:391–396. doi:
40
41 10.1016/j.jhazmat.2011.03.058
42
43
44
45

46
47 Choy KKH, Ko DCK, Cheung CW, et al (2004) Film and intraparticle mass
48
49 transfer during the adsorption of metal ions onto bone char. *J Colloid*
50
51 Interface Sci 271:284–295. doi: 10.1016/j.jcis.2003.12.015
52
53
54
55

56
57 Cui L, Yan J, Li L, et al (2015) Does Biochar Alter the Speciation of Cd and Pb
58
59

1 in Aqueous Solution? BioResources. 10:88–104.

2
3
4 Dodson J (2011) Wheat straw ash and its use as a silica source. Ph.D. thesis
5
6
7 dissertation. University of York.

8
9
10 Foo KY, Hameed BH (2010) Insights into the modeling of adsorption isotherm
11
12
13 systems. Chem Eng J 156:2–10. doi: 10.1016/j.cej.2009.09.013
14
15

16
17 Gillman G, Sumpter E (1986) Modification to the compulsive exchange method
18
19
20 for measuring exchange characteristics of soils. Aust J Soil Res 24:61. doi:
21
22
23 10.1071/SR9860061
24

25
26 Hou D, Al-Tabbaa A (2014) Sustainability: A new imperative in contaminated
27
28
29 land remediation. Environ Sci Policy 39:25–34. doi:
30
31
32 10.1016/j.envsci.2014.02.003
33
34

35
36 Hou D, Ding Z, Li G, et al A Sustainability Assessment Framework for
37
38
39 Agricultural Land Remediation in China.
40
41

42
43 Hou D, Gu Q, Ma F, O'Connell S (2016) Life cycle assessment comparison of
44
45
46 thermal desorption and stabilization/solidification of mercury contaminated
47
48
49 soil on agricultural land. J Clean Prod 139:949–956. doi:
50
51
52 10.1016/j.jclepro.2016.08.108
53

54
55 Hou D, Li F Complexities Surrounding China's Soil Action Plan. L Degrad Dev.
56
57
58

1 Hou D, O'Connor D, Nathanail P, et al (2017a) Integrated GIS and multivariate
2
3 statistical analysis for regional scale assessment of heavy metal soil
4
5 contamination: A critical review.
6
7

8
9
10 Hou D, Qi S, Zhao B, et al (2017b) Incorporating life cycle assessment with
11
12 health risk assessment to select the “greenest” cleanup level for Pb
13
14 contaminated soil. J Clean Prod 162:1157–1168. doi:
15
16 10.1016/j.jclepro.2017.06.135
17
18
19

20
21
22 Inyang MI, Gao B, Yao Y, et al (2015) A Review of Biochar as a Low-Cost
23
24 Adsorbent for Aqueous Heavy Metal Removal. Crit Rev Environ Sci
25
26 Technol 00–00. doi: 10.1080/10643389.2015.1096880
27
28

29
30
31 Jahirul MI, Rasul MG, Chowdhury AA, Ashwath N (2012) Biofuels production
32
33 through biomass pyrolysis- A technological review. Energies 5:4952–5001.
34
35 doi: 10.3390/en5124952
36
37
38

39
40
41 Keiluweit M, Kleber M (2009) Molecular-level interactions in soils and
42
43 sediments: The role of aromatic π -systems. Environ Sci Technol
44
45 43:3421–3429. doi: 10.1021/es8033044
46
47
48

49
50 Keiluweit M, Nico PS, Johnson M, Kleber M (2010) Dynamic molecular
51
52 structure of plant biomass-derived black carbon (biochar). Environ Sci
53
54 Technol 44:1247–1253. doi: 10.1021/es9031419
55
56
57

1 Lehmann J (2007) Bio-energy in the black. *Front Ecol Environ* preprint:1. doi:

2
3 10.1890/060133
4
5

6
7 Li H, Dong X, da Silva EB, et al (2017) Mechanisms of metal sorption by
8

9 biochars: Biochar characteristics and modifications. *Chemosphere*
10

11 178:466–478. doi: 10.1016/j.chemosphere.2017.03.072
12
13

14
15
16 Liu P, Liu WJ, Jiang H, et al (2012a) Modification of bio-char derived from fast
17

18 pyrolysis of biomass and its application in removal of tetracycline from
19

20 aqueous solution. *Bioresour Technol* 121:235–240. doi:
21

22 10.1016/j.biortech.2012.06.085
23
24

25
26
27
28 Liu W, Wang T, Borthwick AGL, et al (2013) Adsorption of Pb²⁺, Cd²⁺, Cu²⁺
29

30 and Cr³⁺ onto titanate nanotubes: Competition and effect of inorganic
31

32 ions. *Sci Total Environ* 456–457:171–180. doi:
33

34 10.1016/j.scitotenv.2013.03.082
35
36

37
38
39
40 Liu Y, Zhao X, Li J, et al (2012b) Characterization of bio-char from pyrolysis of
41

42 wheat straw and its evaluation on methylene blue adsorption. *Desalin*
43

44 *Water Treat* 46:115–123. doi: 10.1080/19443994.2012.677408
45
46

47
48
49
50 Ma F, Peng C, Hou D, et al (2015) Citric acid facilitated thermal treatment: An
51

52 innovative method for the remediation of mercury contaminated soil. *J*
53

54 *Hazard Mater* 300:546–552. doi: 10.1016/j.jhazmat.2015.07.055
55
56

- 1 Ma F, Zhang Q, Xu D, et al (2014) Mercury removal from contaminated soil by
2
3 thermal treatment with FeCl₃ at reduced temperature. Chemosphere
4
5 117:388–393. doi: 10.1016/j.chemosphere.2014.08.012
6
7
8
9
- 10 Mohan D, Kumar H, Sarswat A, et al (2014) Cadmium and lead remediation
11
12 using magnetic oak wood and oak bark fast pyrolysis bio-chars. Chem
13
14 Eng J 236:513–528. doi: 10.1016/j.cej.2013.09.057
15
16
17
18
- 19 Mohan D, Pittman CU, Bricka M, et al (2007) Sorption of arsenic, cadmium,
20
21 and lead by chars produced from fast pyrolysis of wood and bark during
22
23 bio-oil production. J Colloid Interface Sci 310:57–73. doi:
24
25 10.1016/j.jcis.2007.01.020
26
27
28
29
30
- 31 Park J-H, Cho J-S, Ok YS, et al (2015) Comparison of single and competitive
32
33 metal adsorption by pepper stem biochar. Arch Agron Soil Sci
34
35 340:150717092443002. doi: 10.1080/03650340.2015.1074186
36
37
38
39
40
- 41 Qi S, Hou D, Luo J (2017) Optimization of groundwater sampling approach
42
43 under various hydrogeological conditions using a numerical simulation
44
45 model. J Hydrol 552:505–515.
46
47
48
49
- 50 Rees F, Simonnot MO, Morel JL (2014) Short-term effects of biochar on soil
51
52 heavy metal mobility are controlled by intra-particle diffusion and soil pH
53
54 increase. Eur J Soil Sci 65:149–161. doi: 10.1111/ejss.12107
55
56
57
58

- 1 Ronsse F, van Hecke S, Dickinson D, Prins W (2013) Production and
2
3 characterization of slow pyrolysis biochar: influence of feedstock type and
4
5 pyrolysis conditions. *GCB Bioenergy* 5:104–115. doi: 10.1111/gcbb.12018
6
7
8
9
- 10 Saleh ME, El-Refaey AA, Mahmoud AH (2016) Effectiveness of sunflower
11
12 seed husk biochar for removing copper ions from wastewater: a
13
14 comparative study. *Soil Water Res* 11:53–63. doi:
15
16 10.17221/274/2014-SWR
17
18
19
20
21
- 22 Shen Z, Jin F, Wang F, et al (2015) Sorption of lead by Salisbury biochar
23
24 produced from British broadleaf hardwood. *Bioresour Technol* 193:553–
25
26 556. doi: 10.1016/j.biortech.2015.06.111
27
28
29
30
- 31 Shen Z, Som AM, Wang F, et al (2016) Long-term impact of biochar on the
32
33 immobilisation of nickel (II) and zinc (II) and the revegetation of a
34
35 contaminated site. *Sci Total Environ* 542:771–776.
36
37
38
39
40
- 41 Shen Z, Tian D, Zhang X, et al (2017a) Mechanisms of biochar assisted
42
43 immobilization of Pb 2+ by bioapatite in aqueous solution. *Chemosphere*
44
45 190: 260-266. doi: 10.1016/j.chemosphere.2017.09.140
46
47
48
49
- 50 Shen Z, Zhang Y, Jin F, et al (2017b) Qualitative and quantitative
51
52 characterisation of adsorption mechanisms of lead on four biochars. *Sci*
53
54 *Total Environ* 609:1401–1410. doi: 10.1016/j.scitotenv.2017.08.008
55
56
57
58

- 1 Shen Z, Zhang Y, McMillan O, et al (2017c) Characteristics and mechanisms
2
3 of nickel adsorption on biochars produced from wheat straw pellets and
4
5 rice husk. *Environ Sci Pollut Res* 1–11. doi: 10.1007/s11356-017-8847-2
6
7
8
9
- 10 Song Y, Hou D, Zhang J, et al (2018) Environmental and socio-economic
11
12 sustainability appraisal of contaminated land remediation strategies: A
13
14 case study at a mega-site in China. *Sci Total Environ* 610–611:391–401.
15
16
17 doi: 10.1016/j.scitotenv.2017.08.016
18
19
20
21
- 22 Tran HN, You S-J, Chao H-P (2016) Effect of pyrolysis temperatures and times
23
24 on the adsorption of cadmium onto orange peel derived biochar. *Waste*
25
26
27
28 *Manag Res* 34:129–138. doi: 10.1177/0734242X15615698
29
30
- 31 Uchimiya M, Cantrell KB, Hunt PG, et al (2012) Retention of Heavy Metals in a
32
33
34 Typic Kandudult Amended with Different Manure-based Biochars. *J*
35
36
37 *Environ Qual* 41:1138. doi: 10.2134/jeq2011.0115
38
39
40
- 41 Usman A, Sallam A, Zhang M, et al (2016) Sorption Process of Date Palm
42
43
44 Biochar for Aqueous Cd (II) Removal: Efficiency and Mechanisms. *Water*
45
46
47 *Air Soil Pollut*. doi: 10.1007/s11270-016-3161-z
48
49
- 50 Wang Z, Han L, Sun K, et al (2016) Sorption of four hydrophobic organic
51
52
53
54
55
56
57
58
59
60
61
62
63
64
65

1 doi: 10.1016/j.chemosphere.2015.08.042

2
3
4 Zhang H, Chen C, Gray EM, Boyd SE (2017a) Effect of feedstock and
5
6
7 pyrolysis temperature on properties of biochar governing end use efficacy.
8
9
10 Biomass and Bioenergy 105:136–146. doi:
11
12 10.1016/j.biombioe.2017.06.024
13
14

15
16 Zhang P, Lo I, O'Connor D, et al (2017b) High efficiency removal of methylene
17
18
19 blue using SDS surface-modified ZnFe₂O₄ nanoparticles. J Colloid
20
21
22 Interface Sci 508:39–48.
23
24
25
26
27
28
29
30
31
32
33
34
35
36
37
38
39
40
41
42
43
44
45
46
47
48
49
50
51
52
53
54
55
56
57
58